ELSEVIER

Journal of Nuclear Materials 290–293 (2001) 1052–1058

journal of nuclear materials

www.elsevier.nl/locate/jnucmat

Material erosion and erosion products under plasma heat loads typical for ITER hard disruptions

V. Safronov [a,*], N. Arkhipov [a], V. Bakhtin [a], S. Kurkin [a], F. Scaffidi-Argentina [b], D. Toporkov [a], S. Vasenin [a], H. Würz [b], A. Zhitlukhin [a]

[a] *Troitsk Institute for Innovation and Fusion Research, 142092 Troitsk , Moscow region, Russian Federation*
[b] *Forschungszentrum Karlsruhe, P.O. Box 3640, D-76021 Karlsruhe, Germany*

Abstract

Plasma/material interaction has been studied in disruption simulation experiments. Candidate divertor materials were exposed to heat loads expected for tokamak-reactor disruptions. It is shown that sudden evaporation of a thin material layer produces a cloud of vapor plasma, which acts as a thermal shield protecting the surface from further excessive evaporation. In terms of evaporation reduction a shielding factor is above 100. Formation and physical properties of the shielding layer are analyzed. Target plasma converts the incoming energy flux into photon radiation. Radiation from target plasma is so intensive that it may cause erosion of nearby components. Surface damages result not solely from atomic vaporization but also from melt layer splashing for metals and brittle destruction for carbon-based materials. Erosion products are emitted as droplets (metal) and grains (carbon-based material). Melt layer splashing results in greater surface damages than vaporization. A contribution of brittle destruction to net erosion is under investigation now.

Keywords: Plasma disruption; Shielding; Erosion

1. Introduction

During tokamak plasma disruption and during ELMs, the divertor plates are exposed to an intense flow of hot plasma. In tokamak-reactor, divertor heat flux will be so intensive that it can cause severe erosion of plasma facing materials (PFMs). Plasma-induced damage to PFMs is a major concern for safe, successful and reliable reactor operation. Erosion restricts lifetime of divertor components and produces substantial amount of material dust, which being tritiated, radioactive and chemically reactive presents serious problem for a safety. The exact amount and properties of eroded material are critically important to lifetime and safety analysis of tokamak-reactor.

In the next-step device ITER-FEAT, the divertor heat loads are estimated to be $Q_{\mathrm{disr}} = 1$–20 MJ/m^2 for thermal quench phase ($t = 1$–10 ms) of disruption and $Q_{\mathrm{ELM}} = 1$–2 MJ/m^2, $t = 0.1$–1 ms for ELMs [1]. Such energy densities cannot be achieved in current tokamak machines. Therefore, plasma-induced erosion is investigated in laboratory experiments capable to simulate, at least in part, the loading conditions expected for plasma disruption and ELMs.

Tasks of disruption simulation experiments, applied experimental schemes and obtained experimental results are considered in the present paper.

2. Disruption simulation experiments

2.1. Experiment objectives

Disruption simulation experiments are aimed at investigation of material erosion under disruption heat loads expected in future tokamak machines. However

* Corresponding author. Tel.: +7-095 334 5240; fax: +7-095 334 5776.
E-mail address: vsafr@rico.ttk.ru (V. Safronov).

0022-3115/01/$ - see front matter
PII: S0022-3115(00)00662-0

the properties of tokamak plasma and disruption conditions cannot be precisely reproduced in the simulation experiment. It is therefore necessary to develop a comprehensive model including all major physical processes occurring at plasma/material interaction during disruptions and to use this model for extrapolation of experimental results to tokamak condition and for prediction of disruption damages. Such models are developed at several laboratories [2–4].

Objectives of the simulation experiments include:

- study of the physical processes at plasma/material interaction,
- study of erosion mechanisms and material erosion,

at the conditions as close as possible to tokamak disruption. Experimental data are required for the development and validation of appropriate physical models.

Interaction of pulse energetic plasma with solid material results in sudden vaporization of a thin surface layer and produces a cloud of dense vapor plasma. Vapor plasma acts as a thermal shield stopping the plasma stream and protecting the surface from direct action of hot plasma. Target plasma dissipates the incoming energy flux into photon radiation thereby reducing the net power flux reaching the surface. Due to the shielding effect, material vaporization decreases substantially [5].

Shielding effect is a major physical phenomenon to be studied in disruption simulation experiments. Experimental study of this effect includes investigations of the following processes:

- formation, evolution and stability of the shielding layer;
- interaction of pulse energetic plasma with the shielding layer, transformation of hot plasma energy into thermal energy of target plasma and radiation;
- energy transport in the shielding layer;
- material erosion.

Disruption damages to the divertor materials result not solely from atomic vaporization but also from melt layer splashing for metals and brittle destruction for carbon-based materials. Erosion products are emitted as droplets (for metal) and grains (for CBMs) [6]. An important task is to investigate and quantify the mechanisms of material erosion as well as to study erosion products, interaction of eroded particles with plasma and effect of material dust on the shielding layer properties.

Plasma shield converts energy of hot plasma into intense radiation [7], which goes out in all directions from target plasma and may cause erosion of nearby components. This effect should be investigated also.

2.2. Simulation devices

Electron beams, open plasma traps and plasma guns (Table 1) are used to simulate disruption heat loads on PFMs. All simulation devices can produce reactor relevant pulse energy densities. However the shielding layer properties and energy flux reaching the surface depend on many other parameters (particle energy, pulse duration, geometrical factors, etc.) and at identical heat

Table 1
Simulation devices

Facility	Type	Parameters
MK-200UG [8] TRINITI, Troitsk, Russia	Pulsed plasma gun with long magnetic drift tube	Energy density $Q = 15$ MJ/m^2 Pulse duration $t = 40$–50 μs Impact ion energy $E_i = 1.5$ keV Plasma temperature $T_i + T_e = 1$ keV Magnetic field $B = 2$ T
MK-200CUSP [8] TRINITI, Troitsk, Russia	Pulsed plasma gun with magnetic quadrupole	$Q = 2$ MJ/m^2, $t = 15$–20 μs, $E_i = 0.8$ keV, $T_i + T_e = 0.6$ keV, B = 2–3 T
VIKA [9] Efremov Institute, St. Peterburg, Russia	Quasi-stationary plasma gun	$Q = 2$–30 MJ/m^2, $t = 90$–360 μs, $E_i = 0.2$ keV, $T_i + T_e = 10$ eV, B = 0–3 T
QSPA [10] TRINITI, Troitsk, Russia	Quasi-stationary plasma gun	$Q = 5$–10 MJ/m^2, $t = 250$–600 μs, $E_i = 0.1$ keV, $T_i + T_e = 10$ eV, $B = 0$–1 T
QSPA Kh 50 [11] IPP NSC KIPT Kharkov, Ukraine	Quasi-stationary plasma gun	$Q = 10$–40 MJ/m^2, $t = 200$ μs, $E_i = 0.3$ keV, $T_i + T_e = 10$ eV, $B = 0$–2 T
PLADIS [12] Sandia Lab, USA	Quasi-stationary plasma gun	$Q = 0.5$–10 MJ/m^2, $t = 80$–500 μs, $E_i = 0.1$ keV, $T_i + T_e = 10$ eV, $B = 0$
JUDITH [13] KFA Germany	150 keV electron beam	$Q = 5$–10 MJ/m^2, $t = 5$ ms, $E_e = 120$ keV, $B = 0$ T
JEBIS [14] JAERY, Japan	70 keV electron beam	$Q = 2.5$ MJ/m^2, $t = 2$ ms, $E_e = 70$ keV, $B = 0$ T
ITER–FEAT	Tokamak	$Q = 1$–20 MJ/m^2, $t = 1$–10 ms, $E_i s$, $E_e < 10$–20 keV, $B = 5$ T

load a magnitude of erosion can considerably differ at various devices. Therefore the results of disruption simulation experiments should be carefully interpreted and critically examined with respect to relevance to tokamak condition.

E-beam facilities generate electrons with a high energy (100 keV) that is greater than in tokamak plasma (<10–20 keV). Because of high kinetic energy, electrons penetrate considerably deeper into the vapor cloud and material than disruptive plasma. As a result, lower energy is deposited in the vapor cloud and more energy is delivered to the surface causing large erosion. Therefore e-beam devices cannot be applied for experimental modeling of the shielding effect. However, having well-calibrated and controlled parameters these devices (JUDITH, JEBIS) are suitable for testing the materials by pulse heat loads.

The main concern in the use of plasma guns is low directed energy of pulse plasma. Quasi-stationary plasma guns VIKA, QSPA, QSPA-Kh50 and PLADIS produce plasma with kinetic energy of ions $E_i \approx 100$ eV and density $n > 10^{22}$ m^{-3} that differs from tokamak conditions ($E_i < 10$–20 keV, $n < 10^{20}$ m^{-3}). Because of low kinetic energy and large density, a shock wave arises at plasma/target interaction. Shock wave causes deceleration of the stream and energy flux reaching the surface decreases not solely due to vapor shielding effect but because of self-shielding effect also. This effect is important for experiment with magnetic field, when well-confined cloud of stopped hydrogen plasma produces additional screening to the surface. Though the surface heat load significantly decreases, it is high enough to cause material erosion. Quasi-stationary plasma guns are suitable to study effects of long-term plasma action on PFMs.

Pulsed plasma gun MK-200UG generates plasma with ion energy $E_i \geqslant 1$ keV and density $n = 1$–5×10^{21} m^{-3}. Self-shielding effect is practically negligible. The facility is equipped with magnetic field. Target materials can be tested at perpendicular and inclined plasma impact. Disadvantage of MK-200UG is a short pulse duration $t = (40$–$50)$ μs. Meanwhile the facility is well suited to simulate early stages of tokamak disruption and to study formation and properties of the plasma shield.

3. Experimental results

3.1. Shielding effect

Shielding effect has been studied at the all plasma devices from Table 1. Detailed investigations of plasma shield properties were performed at MK-200 facility. There were studied different target materials including tungsten and graphite. Targets were exposed to normal and inclined plasma impact as well as to radiation from target plasma (Fig. 1). Optical interferometers, visible and absolutely calibrated VUV spectroscopes laser scattering diagnostics, calorimeters, bolometers, pressure sensors and multi-frame cameras have been used for the measurements in plasma shield.

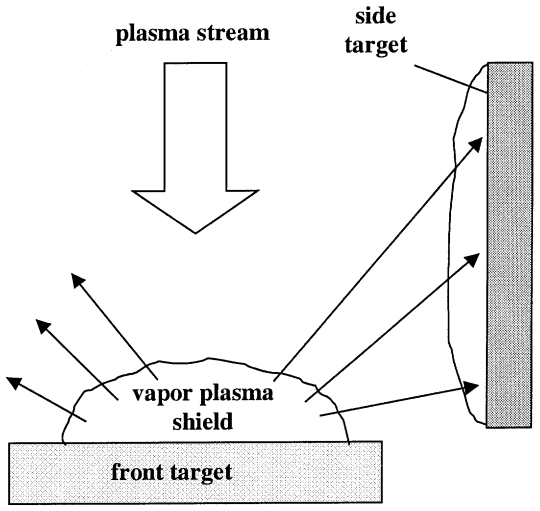

Fig. 1. General scheme of experiment.

3.1.1. Plasma shield formation and dynamics

Time of plasma shield formation depends on plasma heat flux: the higher heat flux the less time. For graphite target, a cloud of dense ($n > 10^{23}$ m^{-3}) carbon plasma arises after $t = 5$ μs at heat flux $W = 10$ GW/m^2 [10] while at $W \geqslant 100$ GW/m^2, it is formed within 1 μs [15]. This time is much less than a whole time of plasma/material interaction. Dense target plasma arises at early stage of interaction process and then protects the surface against action of energetic plasma.

Magnetic field affects motion of target plasma. At perpendicular plasma impact (Fig. 1) target plasma expands along the magnetic field lines upward the plasma stream. Transverse motion is basically inhibited because of magnetic field [16]. In experiments without magnetic field [10], target plasma flows around the target that causes loss of vaporized material and reduction of shielding effect. At inclined plasma incidence, an oblique magnetic field does not stop fully a transverse motion and target plasma drifts downwards the tilted surface [8,17].

Parameters and dynamics of target plasma depend on a kind of target material. Low Z target plasma (graphite, boron nitride and plexiglas) expands from the surface at large distances. For high Z materials (tungsten, molybdenum, copper) target plasma is localized near the surface [15,16].

In experiment with perpendicular targets exposed to plasma heat flux $W = 100$–300 GW/m^2 [18,19], a velocity was measured to be 3–4×10^4 m/s for carbon

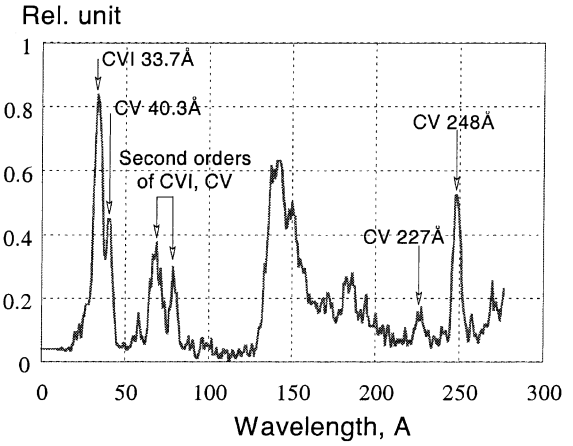

Fig. 2. Spectrum of carbon target plasma at time $t = 10.5$ μs. (measured at 2 cm from MPG-8 graphite exposed to plasma power density 100 GW/m^2).

plasma, and 3–4 $\times$ 10^4 m/s for copper plasma. Tungsten plasma was localized in the layer of 2–3 cm thickness during a whole interaction process.

3.1.2. Plasma shield properties

Vapor cloud consists of highly stripped ions of target material [20]. Fig. 2 shows spectrum of radiation from carbon target plasma (MK-200, $W = 100$ GW/m^2). Radiation of helium-like C^{+4} ions (CV40.3 Å) and hydrogen-like C^{+5} ions (CVI33.7 Å) indicates existence of high temperature carbon plasma. Essential part of tungsten plasma radiation belongs also to VUV spectral band $\lambda < 400$ Å [21].

According to direct measurements [22], a temperature in carbon plasma is about $t_e = 40$ eV at 1 cm distance from the surface and increases to $t_e = 60$–90 eV at 10 cm distance. Temperature in tungsten plasma is less than in carbon plasma ($t_e \leqslant 20$ eV at 1 cm).

Because of large temperature gradient, electron thermal conductivity contributes considerably to the surface heat flux. Electron heat flux is the most important for low Z materials. For high Z material, radiation transport and radiation heat flux become dominant [23].

3.1.3. Energy balance and material vaporization

Energy of incident hot plasma, energy of radiation from target plasma, target heating and amount of vaporized material have been measured at MK-200 for analysis of energy balance.

It is found that target plasma shield dissipates the incident energy ($Q = 15$ MJ/m^2) practically completely into outgoing radiation and radiative loss is dominant in the energy balance [24]. Because of radiative loss, energy reaching the target surface becomes much smaller than the incident energy.

For graphite target, energy consumed for target heating was measured to be $Q_h = 300$ kJ/m^2. Erosion is 0.4 μm that corresponds to energy $Q_v = 30$ kJ/m^2 spent for graphite vaporization. Thus a great bulk of incident energy is lost in the plasma shield. In terms of evaporation reduction a shielding factor Q/Q_v is 500! With no shielding effect, when the incident energy $Q = 15$ MJ/m^2 is consumed completely for graphite heating and vaporization, an erosion rate would be about 200 μm/shot.

Table 2 shows maximum graphite erosion measured in plasma gun experiments. Erosion was measured after multiple exposures and one-shot erosion was evaluated.

Energy dependence of erosion is not linear. Increase of impact energy density by a factor of 7.5 (MK-200) results in increase of erosion by a factor of 1.6 only.

In VIKA experiment [25] there was found that erosion increases with plasma pulse duration. One can see that quasi-stationary plasma guns produce greater erosion than pulsed guns. However erosion was measured at quasi-stationary guns without magnetic field and these experiments give upper estimation for erosion. At QSPA facility the ere was studied effect of magnetic field on graphite erosion [10]. Erosion was measured to be 1.5 μm/shot in experiment without magnetic field. In experiments with magnetic field, erosion was not found at all because of very small magnitude.

Erosion magnitudes (Table 2) were measured at different facilities under different experimental conditions. That is important, all these experiments show very small erosion thereby indicating a high efficiency of the plasma shield. For all the experiments a shielding factor is above 100 excepting QSPA where it equals to 60.

Angular dependence of graphite erosion was studied at MK-200UG. Perpendicular (0°tilted) and tilted at the angle $\alpha = 30, 50, 70°$ targets were examined. Maximum erosion rate (0.4 μm/shot) was measured at perpendicular target. Erosion rate decreases with target inclination (but less quickly than plasma heat load $Q_\alpha = Q \cos\alpha$ and it becomes 0.22 μm/shot at 70° tilted target (Fig. 3). These measurements were done for 'large' targets, which overlap fully the plasma stream. At 'small' targets the erosion rate increases essentially with sample inclination [8]. Incident plasma blows away target plasma from 'small' tilted surface that causes loss of vaporized material and reduction of shielding effect.

Table 2
Graphite erosion for one shot

Facility	Energy (MJ/m^2)/ pulse duration(μs)	Erosion (μm)
MK-200UG	15/50	0.4
MK-200CUSP	2/20	0.25
VIKA	30/360	2.3
QSPA	7/600	1.5
QSPA Kh 50	40/200	1.6

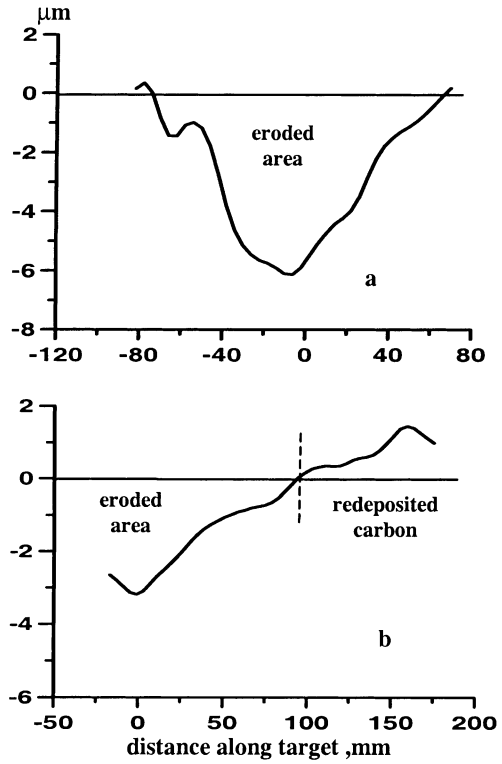

Fig. 3. Surface profile on perpendicular (a) and 20°-tilted (b) MPG-8 graphite plates exposed to 15 plasma discharges at energy density 15 MJ/m^2. (stream axis – $x = 0$).

3.1.4. Effect of target plasma radiation on nearby components

Intensity and spatial distribution of radiation from target plasma depend on a kind of material (Fig. 4). Radiative loss from carbon plasma is distributed at whole length of target plasma column. For tungsten, the radiative loss is strongly peaked close to the target. A half of the incident energy is re-radiated in 1.5–2 cm near-surface layer. Tungsten plasma radiation is so intensive that it may cause erosion of nearby components.

In [26] there was studied graphite erosion induced by tungsten plasma radiation. Front tungsten target was exposed to plasma stream (Fig. 1). Side graphite target was placed outside plasma stream at 10 cm distance from the stream axis and it was exposed to radiation from tungsten plasma. Radiation heat load Q_r was measured on side target by use of radiation calorimeter. Heat load was varied in the range of $Q_r = 0.2$–1 MJ/m^2 with unaltered pulse duration 40 μs.

Tungsten plasma radiation causes strong erosion of side graphite. Erosion is proportional to radiation flux. At $Q_r = 1$ MJ/m^2 the erosion rate is 0.35 μm/shot that is similar to graphite erosion (0.4 μm/shot) caused by pulse plasma at $Q_{pl} = 15$ MJ/cm^2. Therefore a shielding efficiency of carbon plasma against action of tungsten

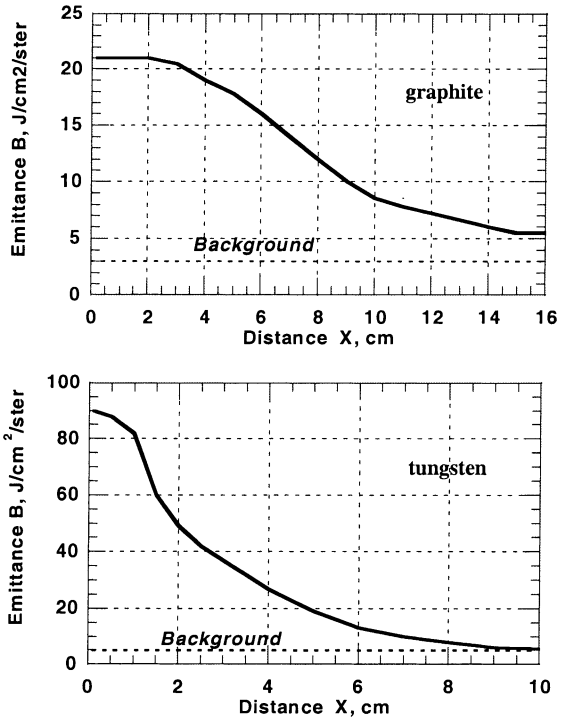

Fig. 4. Radiative loss from target plasma shield.

plasma radiation is much lower than against action of hot plasma. It is explained by the fact that carbon target plasma is transparent for tungsten radiation and lower energy is deposited in the vapor cloud and more energy is delivered to the surface than in plasma experiment.

4. Erosion mechanisms and erosion products

Laboratory experiments have contributed significantly in understanding of the shielding effect and have supplied experimental data for validation of numerical models [2–4]. Recently developed one- and two-dimensional numerical codes FOREV [2] quite well reproduce the results of simulation experiments [7,27–29] including MHD movement of target plasma, plasma temperature and density evolution, spectral and spatial distribution of radiation flux, etc. Applied to tokamak disruption this numerical model can determine disruptive heat fluxes on PFM's and thus can evaluate a mass of evaporated material. However material damages result not solely from vaporization but also from melt layer splashing for metals and brittle destruction for CBMs. The lasts demand extra investigation.

4.1. Carbon-based materials

Erosion of CBMs results from vaporization and brittle destruction. Brittle destruction plays a primary

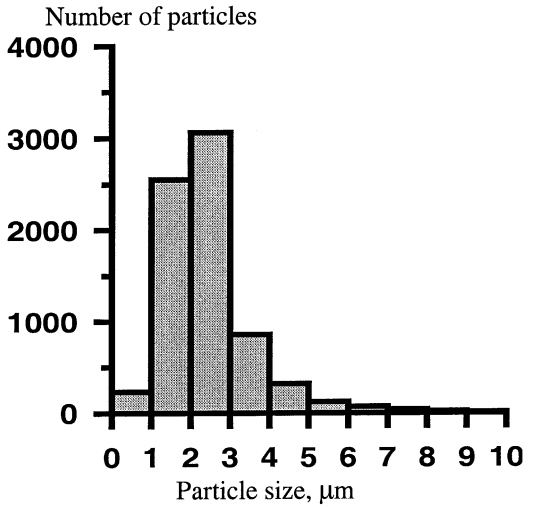

Fig. 5. Size distribution of carbon particles eroded from MPG-8 graphite target at plasma heat load 15 MJ/m^2.

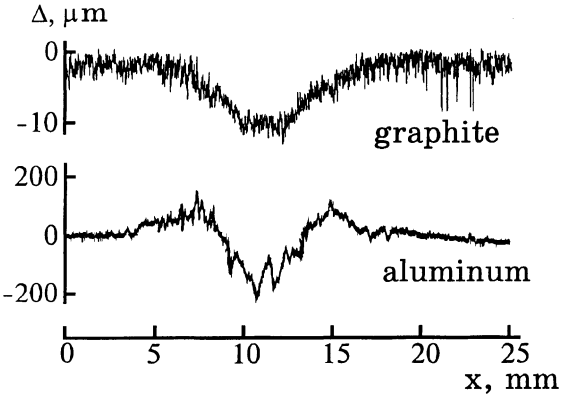

Fig. 6. Erosion profiles (MPG-8 graphite – 40 shots, aluminum – 18 shots at plasma heat load 2 MJ/m^2).

role in e-beam experiments [30] where erosion products are emitted mainly as particles. In plasma experiments, eroded carbon particles are observed also (Fig. 5) and therefore macroscopic destruction presents a real mechanism of plasma-induced erosion. However it is fully unclear now whether brittle destruction can cause greater erosion of CBMs than vaporization because emitted particles are vaporized quickly in plasma shield and it results in additional target screening. Investigations are just started in this field.

Evaporated carbon produces redeposited carbon layers on all components of vacuum vessel including target surface [31]. Amount of redeposited material is negligible on perpendicular target but increases with target inclination (Fig. 3). It is explained by different dynamics of eroded material at perpendicular and tilted surfaces.

4.2. Metal targets

Plasma shield reduces extremely material vaporization, however it cannot stop melting. Pulse plasma impact results in formation of melt layer on metal target. Melt layer is subjected to the action of different forces which can cause a severe melt layer loss. Fig. 6 shows erosion profiles for graphite and aluminum from MK-200CUSP experiment. Erosion rate of aluminum (10 μm/shot) is much greater for graphite (0.25 μm/shot). Large erosion of aluminum results from melt layer splashing. Because of pressure gradient, melt metal is removed from erosion crater thus producing mountains around the crater. Contribution of evaporation is negligible to net aluminum erosion.

Melt layer erosion results from different mechanisms such as melt layer motion, volumetric boiling, hydrodynamical instabilities, etc. These mechanisms have been partly analyzed in [32], however now there is no reliable model capable to evaluate erosion for metal.

At present the most solid experimental data are obtained for light metals (aluminum and beryllium). Erosion of light metals is 1–2 order of magnitude greater than erosion of CBMs at identical conditions [12,13,18,25,33]. Large fraction of erosion products is emitted as 1–10 μm droplets [33]. Because of great melt layer erosion, light metals cannot withstand to disruption heat flux.

Tungsten demonstrates low erosion. Table 3 represents W erosion measured in disruption simulation experiments. The measurements were done by sample weighting. One can see that tungsten erosion is below 1 μm/shot that is similar to graphite erosion. However in contrast to graphite, tungsten show severe surface cracking [34]. The following thermal cycling test with heat load 20 MW/m^2 [35] causes further cracking including formation of volumetrical cracks for the majority of tungsten grades. W–5Re–0.1ZrC alloy shows the best performance.

Experiments with tungsten are still too scarce to draw final conclusions on the mechanisms of tungsten erosion and their dependence on experimental conditions.

Table 3
Tungsten erosion for one shot

Facility	Energy(MJ/m^2)/ pulse duration(μs)	Erosion (μm)
MK-200UG	15/50	0.1
MK-200CUSP	2/20	0.3
VIKA	30/360	0.7
QSPA	7/600	0.9

5. Summary

Plasma/material interaction, material erosion and erosion products have been studied in disruption simulation experiments.

At plasma heat fluxes 10–100 GW/m^2, dense target plasma arises at irradiated surface within 1–5 μs. Target plasma dissipates the incoming energy flux into radiation and effectively shields the surface from excessive evaporation. Erosion of graphite and tungsten is limited to 1–2 μm at plasma energy density 2–40 MJ/m^2. In terms of evaporation reduction a shielding factor is above 100.

Plasma shield properties (density, temperature, spectrum and intensity of radiation, etc.) have been investigated and there was produced experimental database for validation of numerical models.

Tungsten plasma radiation causes strong erosion of side graphite wall. At $Q_r = 1$ MJ/m^2, graphite erosion is 0.35 μm that is similar to graphite erosion (0.4 μm) caused by plasma pulse at $Q_{pl} = 15$ MJ/m^2.

CBMs erosion results from vaporization and brittle destruction. Erosion products contain micron grains. Contribution of brittle destruction to net erosion is unknown now.

Erosion of light metals (Al, Be) is 1–2 order of magnitude greater than erosion of CBMs. The enhanced erosion results from melt layer splashing.

Tungsten erosion is below 1 μm at plasma heat load 2–30 MJ/m^2. Surface damages are caused mainly by surface cracking.

Present knowledge on brittle destruction and mechanisms of metal damages is insufficient to extrapolate the available data to tokamak conditions. Investigation should be continued in these fields.

References

[1] M. Shimada et al., in: Proceedings of the 10th Toki International Conference, Toki-shi, Japan, 18–21 January 2000.
[2] H. Wuerz et al., Hot plasma target interaction and quantification of erosion of the ITER slot divertor during disruption and ELMs, Forschunszentrum Karlsruhe Report/FZKA 6198, 1999.
[3] A. Hassanein, I. Konkashbaev, Plasma Dev. Oper. 5 (1998) 297.
[4] Lalousis et al., in: Proceedings of the 22nd EPS Conference on Controlled Fusion and Plasma Physics, Bournemouth, UK, vol. 19C, 3–7 July 1997, p. 2285.
[5] A. Sestero, Nucl. Fus. 17 (1977) 171.
[6] M. Guseva et al., J. Nucl. Mater. 220–222 (1995) 957.
[7] H. Wuerz et al., Fus. Technol. 30 (1996) 739.
[8] N. Arkhipov et al., J. Nucl. Mater. 233–237 (1996) 767.
[9] V. Kozhevin et al., Fus. Eng. Des. 28 (1993) 157.
[10] V. Belan et al., J. Nucl. Mater. 241–243 (1996) 763.
[11] V. Chebotarev et al., J. Nucl. Mater. 233–237 (1996) 736.
[12] J. Crawford et al., J. Nucl. Mater. 203 (1993) 280.
[13] J. Linke et al., J. Nucl. Mater. 212–215 (1994) 1195.
[14] K. Nakamura et al., J. Nucl. Mater. 196–198 (1992) 627.
[15] N. Arkhipov et al., in: Proceedings of the 17th SOFT, vol. 1, Rome, Italy, 14–18 September 1992, p. 171.
[16] N. Arkhipov et al., Plasma Phys. Rep. 25 (3) (1999) 236.
[17] N.P. Arkhipov et al., in: Proceedings of the 26th EPS Conference on Controlled Fusion and Plasma Physics, Part 2, Maastricht, Netherlands, 1999, p. 837.
[18] N. Arkhipov et al., in: Proceedings of the 18th SOFT, vol. 1, Karlsruhe, Germany, 22–26 August 1994, p. 463.
[19] N. Arkhipov et al., in: Proceedings of the 19th SOFT, vol. 1, Lisboa, Portugal, 16–20 September 1996, p. 507.
[20] N. Arkhipov et al., J. Nucl. Mater. 266–269 (1999) 751.
[21] N. Arkhipov et al., in: Proceedings of the 18th SOFT, vol. 1, Karlsruhe, Germany, 22 – 26 August 1994, p. 395.
[22] N. Arkhipov et al., Plasma Phys. Rep. 24 (4) (1998) 309.
[23] S. Vasenin et al., Target plasma radiation in disruption simulation experiment, TRINITI Troitsk Report/ TRINITI 0011-A, 1995.
[24] V. Safronov et al., Disruption simulation experiments at MK-200 facility, in: Workshop on Disruption Erosion, St. Peterburg, Russia, 24–26 November 1997.
[25] V. Litunovsky et al., in: Proceedings of the 20th SOFT, vol. 1, Marseille, France, 7–11 Septemer 1998, p. 59.
[26] S. Vasenin et al., in: Proceedings of the XIII International Conference on Ion and Surface Interaction, vol. 2, Moscow, Russia, 1–5 September 1997, p. 178.
[27] H. Würz et al., J. Nucl. Mater. 212–215 (1994) 1349.
[28] H. Würz et al., Fus. Technol. 32 (1997) 45.
[29] H. Würz et al., in: Proceedings of the ISFNT-5, Rome, Italy, September 1999, Fus. Eng. Des., submitted.
[30] J. Linke et al., O-6.1, these Proceedings.
[31] F. Scaffidi-Argentina et al., in: Proceedings of the ICFRM-9, Colorado Springs, USA, 10–25 October 1999.
[32] A. Hassanein et al., J. Nucl. Mater. 241–243 (1997) 288.
[33] V. Belan et al., in: Proceedings of the 20th SOFT, vol. 1, Marseille, France, 7–11 September 1998, p. 101.
[34] A. Makhankov et al., in: Proceedings of the 20th SOFT, vol. 1, Marseille, France, 7–11 September 1998, p. 267.
[35] A. Makhankov et al., P-3.53, these Proceedings.